Icarus 202 (2009) 429–443

Contents lists available at ScienceDirect

Icarus

www.elsevier.com/locate/icarus

Towards self-consistent modeling of the martian dichotomy: The influence of one-ridge convection on crustal thickness distribution

Tobias Keller *, Paul J. Tackley

Institute of Geophysics, Sonneggstrasse 5, ETH Zurich, 8092 Zurich, Switzerland

ARTICLE INFO

Article history:
Received 5 November 2008
Revised 5 March 2009
Accepted 23 March 2009
Available online 27 March 2009

Keywords:
Geophysics
Planetary dynamics
Mars

ABSTRACT

In order to find an explanation for the origin of the martian crustal dichotomy, a number of recent papers have examined the effect of layered viscosity on the evolution of a degree-1 mantle convection, e.g. Roberts and Zhong [Roberts, J.H., Zhong, S., 2006. J. Geophys. Res. 111. E06013] and Yoshida and Kageyama [Yoshida, M., Kageyama, A., 2006. J. Geophys. Res. 111, doi:10.1029/2005JB003905. B03412]. It was found that a mid-mantle viscosity jump, combined with highly temperature- and depth-dependent rheology, are effective in developing a degree-1 convection within a short timescale. Such a layered viscosity profile could be justified by martian mineralogy. However, the effect of a degree-1 convective planform on the crustal thickness distribution has not yet been demonstrated. It is not obvious whether a thinner crust, due to sublithospheric erosion and crustal thinning, or a thicker crust, due to enhanced crustal production, would form above the hemisphere of mantle upwelling. Also, the general shape of the dichotomy, which is not strictly hemispherical, has not yet been fully investigated. Here we propose a model of the crustal patterns produced by numerical simulations of martian mantle convection, using the finite-volume multigrid code StagYY [Tackley, P.J., 2008. Phys. Earth Planet. Int. 107, 7–18, doi:10.1016/j.pepi.2008.08.005] A self-consistent treatment of melting, crustal formation and chemical differentiation has been added to models of three-dimensional thermal convection. This allows us to obtain global maps of the crustal thickness distribution as it evolves with time. The obtained results demonstrate that it is indeed possible to form a crustal dichotomy as a consequence of near degree-1 mantle convection early in Mars' history. We find that some of the observed patterns show intriguing first order similarities to the elliptical shape of the martian dichotomy. In all models, the region of thick crust is located over the region of mantle upwelling, which itself is a ridge-like structure spread over roughly one half of the planet, a planform we describe as "one-ridge convection."

1. Introduction

One of the most striking features of the martian surface is its crustal dichotomy, i.e. the fact that the planet shows a more or less hemispherical contrast in topography, crustal thickness and crater density. Since this surprising feature of the martian crust was first identified by the Mariner 9 spacecraft (Hartmann, 1973), both endogenic, as for example in Wise et al. (1979), Sleep (1994) and Zhong and Zuber (2001), as well as exogenic processes have been proposed to explain its origin. Exogenic explanations suggest single (Wilhelms and Squyres, 1984) or multiple (Frey and Schultz, 1988) large impacts. Two recent studies addressed this issue and showed that it would be possible to explain the elliptical shape of the dichotomy through one giant impact (Marinova et al., 2008; Nimmo et al., 2008). However, an impact origin may lead to certain difficulties in explaining recent Mars Global Surveyor observations indicating a gradual pole to pole variation in topography and crustal thickness rather than a sudden jump as expected for an impact origin (Zuber, 2001).

In this study we follow on from a number of recent papers to investigate the early evolution of a low-degree convection as a possible explanation for the observed features of the martian crust. Based on martian stratigraphy derived from crater density analysis, it was suggested that the age of the dichotomy reaches back into the Early Noachian, the oldest epoch of the planet's history (Nimmo and Tanaka, 2005). Thus, the bulk of the martian crust as well as the dichotomy itself are thought to have formed largely during the first 300 Myr after core-formation. There are indications, such as buried impact craters, which suggest that the basement crust underlying the smooth sediments of the northern hemisphere is of a similar age as the southern crust (Watters et al., 2006; Frey et al., 2002).

In a recent study, Roberts and Zhong (2006) showed that it is possible to obtain a reduction of convective degree to $l = 1$ in only a few hundred million years by assuming a mid-mantle viscosity jump and a relatively low viscosity upper mantle. The

* Corresponding author.
E-mail address: keller@erdw.ethz.ch (T. Keller).

0019-1035/$ – see front matter
doi:10.1016/j.icarus.2009.03.029

general effect of layered viscosity profiles on inducing low degree mantle convection in Earth-like planets have been discussed by several studies such as Tackley (1996a), Bunge et al. (1996) and Yoshida and Kageyama (2006). It was found that strongly depth- and temperature-dependent viscosity in terrestrial planets is a reliable mechanism to reduce convective degree. Another possible explanation for a reduction of the number of plumes is an endothermic phase transition to perovskite in the lowermost mantle of Mars, which also has a stabilizing effect on the thermal boundary layer above the CMB (Harder and Christensen, 1996; Harder, 1998). A deep mantle perovskite transition, however, is not fully supported by all models of martian interior (Sohl and Spohn, 1997) and therefore we will concentrate our study on the effect of a layered viscosity profile.

In order to focus on the mechanisms of crust formation and the crustal thickness distribution produced by low-degree convection, we limit this study to a rather narrow range of parameters, suggested by studies like Roberts and Zhong (2006) to produce low-degree convective planforms. Their study also showed that for a considerable range of viscosity parameters, the number of plumes was not reduced to one single plume. Instead, a stable ridge-shaped upwelling was obtained, the surface expression of which we expect to be close to elliptical in shape (Andrews-Hanna et al., 2008) and could therefore serve as a possible mechanism leading to an elliptically shaped dichotomy. We will call this type of convective planform one-ridge convection in analogy to the commonly used term one-plume convection.

Since Mars, like all terrestrial planets except Earth, lacks plate tectonics and is in a rigid-lid regime, the convection would generally be dominated by small scale downwellings dropping from beneath the stable lithosphere. A high viscosity lower mantle, however, will lead to only a small number of upwellings, which in the end will be collected into one single upwelling region. This feature will eventually overrule the influence of small scale downwellings typical for a rigid-lid. The physical reason for this transition in convective degree to occur is to be found in the partially decoupled convective behavior caused by the viscosity layering (Buffet et al., 1994). As the characteristic wavelength of convection depends strongly on the vertical viscosity structure, the dominant wavelength of convection in the upper mantle will be significantly shorter than in the lower mantle (Ramberg, 1967). Due to bottom heating, the low-degree upwelling, however, develops enough momentum to overrule the small-scale structures in the upper mantle. As a justification for a mid-mantle viscosity jump, only few explanations have been proposed so far, e.g. Zhong and Zuber (2001), suggesting the presence of a weak asthenosphere caused by partial melting of the upper mantle. We do not follow the same approach, since, in our models, partial melting is constrained to a rather thin band below the lithosphere and it does not occur evenly throughout the mantle. Thus it does not appear to be a viable option to globally influence the pattern of convection. Instead, we introduce a mid-mantle viscosity jump linked to the martian mineralogical transition zone below 1000 km depth, which is discussed into more detail below.

With a low-degree convective planform seemingly being a reasonable assumption for physical conditions in the martian mantle, it still remains to be demonstrated whether this convective pattern would indeed produce the observed distribution of crustal thickness on the planet's surface. In order to investigate the evolution of crust formation in space and time, we added a self-consistent treatment of melting, chemical differentiation and fractionation of heat producing elements as well as of melt extraction and eruption to models of mantle convection. The investigation and discussion of the coupling of melting and crust formation to the thermal evolution as well as the evolution of crustal thickness in space and time thus will be the main foci of this study.

2. Model and methods

2.1. Physical model

To compute thermo-chemical convection in three-dimensional spherical geometry, the finite volume multigrid code StagYY was used. Spherical geometry is modeled using the so-called yin–yang grid, consisting of two identically formed half-grids, each similar to a low-latitude part of a polar coordinate grid (Kageyama and Sato, 2004). The physical model includes a self-consistent treatment to allow for melting, chemical differentiation, fractionation of heat producing elements into the crust and multimineralogical phase transitions. To account for the nondiffusive nature of compositional variations, chemical tracers are used to track the change of local composition with time. Features specific to this study have been added to the more general discussion of the code given in previous publications, e.g. Tackley (2008) and Nakagawa and Tackley (2005).

2.2. Equations

In StagYY, the infinite Prandtl number and compressible anelastic approximations are applied. The equations, nondimensionalized to the mantle depth D, thermal diffusion time-scale D^2/κ (where κ is the thermal diffusivity), and superadiabatic temperature drop ΔT_{sa}, are:

1. Conservation of mass

$$\vec{\nabla}\cdot(\bar{\rho}\vec{v}) = 0. \tag{1}$$

2. Conservation of momentum

$$\vec{\nabla}\cdot\left[\eta\left(v_{i,j}+v_{j,i}-\frac{2}{3}v_{k,k}\delta_{ij}\right)\right]-\vec{\nabla}p = \frac{Ra\vec{\hat{z}}\rho(C,z,T)}{\Delta\rho_{\mathrm{thermal}}}. \tag{2}$$

3. Conservation of energy

$$\bar{\rho}C_p\frac{DT}{Dt} = -Di_s\bar{\alpha}\bar{\rho}Tv_z+\vec{\nabla}(\bar{k}\nabla T)+H_R+H_S+H_{\mathrm{Ph}}. \tag{3}$$

4. Conservation of bulk chemistry

$$\frac{\partial C}{\partial t} = -\vec{v}\nabla C. \tag{4}$$

The two nondimensional numbers governing the equations of convection are:

1. Surface dissipation number Di_s

$$Di_s = \frac{\alpha_s g D}{C_p}. \tag{5}$$

2. Reference Rayleigh number Ra

$$Ra = \frac{\rho_s g\alpha_s\Delta T_{\mathrm{sa}}D^3}{\eta(T,z)\kappa_s}. \tag{6}$$

The energy equation is given in its full form, including convection, diffusion, adiabatic effects and three source terms including internal heating, dissipation or shear heating and latent heat of phase transitions defined as follows.

Radioactive heating (discussed into more detail below).

$$H_R = \bar{\rho}H. \tag{7}$$

Viscous dissipation, obtained by multiplying the strain rate with the stress tensor.

$$H_S = \frac{Di_s}{Ra}\eta\left(v_{i,j}+v_{j,i}-\frac{2}{3}v_{k,k}\delta_{ij}\right)v_{i,j}. \tag{8}$$

Table 1
Physical parameters for Mars.

Parameter	Symb.	Value	Units
Depth of mantle	D	1700	km
Planet radius	R_c	3400	km
Superadiabatic T-drop	ΔT_{sa}	2000	K
Surface temperature	T_s	200	K
Mantle density	ρ_s	3500	$kg\,m^{-3}$
Surface gravity	g_s	3.72	$m\,s^{-2}$
Surface expansivity	α_s	3.0×10^{-5}	K^{-1}
Surface conductivity	k_s	4.2	$W\,m^{-1}\,K^{-1}$
Surface diffusivity	κ_s	1.0×10^{-6}	$m^2\,s^{-1}$
Heat capacity	C_p	1200	$J\,kg^{-1}\,K^{-1}$
Activation energy	E_η	200	$kJ\,mol^{-1}\ K^{-1}$
Activation volume	V_η	4.5	$cm^3\,mol^{-1}$
Latent heat of melting	L	550	$J\,kg^{-1}$
Internal heating	H_{init}	2.0857×10^{-11}	$W\ kg^{-1}$
Heating half-life	$\tau_{1/2}$	2.25	Gyr
Crust enrichment factor	Λ	10	–
Surf. dissipation number	Di_s	0.158	–

Latent heat release or consumption of mineralogical phase transitions summed up over all mineral phases.

$$H_{Ph} = C_p \frac{Di_s T}{\bar{\rho}} \sum_{i=1}^{nphase} f_i P_i \frac{d\Gamma_i}{dz} v_z. \tag{9}$$

The variables are temperature T, composition C, velocity $\vec{v}$, and pressure p. The governing parameters are Rayleigh number Ra, internal heating rate H, and surface dissipation number Di_s. Material properties with overbars (density $\bar{\rho}$, thermal expansivity $\bar{\alpha}$ and thermal conductivity $\bar{k}$) vary with depth only. Specific heat capacity C_p is held constant, $\Delta\rho_{thermal}$ is the fractional density variation with temperature ($= \alpha_{dim.} \cdot \Delta T_{dim.}$) and $\rho(C, z, T)$ is the density function depending on composition, depth and temperature. $\vec{\hat{z}}$ is the unit vector in the vertical direction and g is the gravitational acceleration. For the ith phase change, P_i is the phase buoyancy parameter, f_i is the fraction of the relevant mineralogical component in the assemblage and Γ_i is the depth-dependent phase function. Table 1 lists the physical parameters for Mars used in our models.

Values of density ρ, thermal expansivity α, thermal diffusivity κ and thermal conductivity k vary with depth due to pressure, temperature and the mineralogical phase transitions implemented in this model. The composition-dependence of density in specific will be discussed in the section on the chemical model. Thermal expansivity α decreases with depth, whereas both conductivity k and thermal diffusivity κ increase with depth. The exact curves chosen as reference state are given in Fig. 1, how these are calculated is discussed in Tackley (1996b).

The top and bottom boundary conditions are free slip and isothermal. Cooling of the core due to heat conducted into the mantle is accounted for using a parametrized model in which the CMB temperature decreases according to the amount of heat removed during one timestep (Xie and Tackley, 2004; Steinbach and Yuen, 1994). The initial CMB temperature depends on the imposed initial temperature field which is governed by the chosen superadiabatic temperature drop ΔT_{sa}. The thermal initial conditions are set up using thermal boundary layers at the surface and the CMB, an internal mantle temperature between 1500 and 1600 K and a total superadiabatic temperature-drop of 2000 K over the mantle. Random perturbations with an amplitude of 20 K are added to the initial T-field.

2.3. Heat producing elements

Since the enrichment of heat producing elements in crustal materials has a significant influence on the thermal evolution of the planet's interior and thus also influences the crustal growth (Hauck and Phillips, 2002), heat producing elements are assumed to fractionate into the crust with a factor of $\Lambda = 10$ according to the linear relationship

$$H(C) = H_{mean} \frac{1 + C(\Lambda - 1)}{1 + C_{mean}(\Lambda - 1)}.$$

The internal heat production in basaltic crust ($C = 1$) will consequently be increased by a factor of 10 compared to depleted mantle composition ($C = 0$). C_{mean} is the value of mean composition, which stays constant over the whole domain in order to satisfy conservation of bulk chemistry. The value for the mean internal heating H_{mean} is derived from the present chondritic heating rate $H_{chondritic} = 5.2034 \times 10^{-12}\ W\,kg^{-1}$. It decays exponentially with time with a half-life of $\tau_{1/2} = 2.247$ Ga, a value derived from the half-lifes of chondritic radiogenic isotopes. Thus, our models start off with an initially more intense heating of $H_{init} = 2.0857 \times 10^{-11}\ W\,kg^{-1}$. These values compare very well to values derived specifically for Mars as in Wänke and Dreibus (1994).

2.4. Chemical model, melting and eruption

To track compositional changes in the mantle, a two-component chemical system is assumed with a variable C going from $C = 0$ for peridotite to $C = 1$ for basaltic crust/eclogite. The value of C represents the fraction of crustal material in the mantle and is initialized at $C_{mean} = 0.25$ everywhere. As the condition of conservation of bulk composition is maintained, this value of C_{mean} will stay constant over the whole domain, whereas local values of C change due to melting and eruption. The chosen value for C_{mean} is similar to values used in parametrized models with coupled convection and melting done by Breuer and Spohn (2006). It corresponds to a potential crustal thickness of 280 km and approximately represents the volume of basaltic crust that can be produced from a pyrolite mantle by melting the garnet/pyroxene fraction (McKenzie and Bickle, 1988). Basaltic crust is formed self-consistently by melting, differentiation and eruption, which is calculated as a separate substep to solving Eqs. (1)–(4). The compositional model furthermore contains a simplified description of the two main mineral systems in the martian mantle, olivine and garnet/pyroxene. The total fractions of both mineral systems in our models are chosen to represent estimates of martian mantle mineralogy based on SNC meteorites as given by Bertka and Fei (1997), i.e. $f_{ol} = 0.55$ and $f_{gt\text{–}px} = 1 - f_{ol} = 0.45$. The fraction of olivine in harzburgite thus will be 0.733. These mineral fractions also determine the composition-dependence of density. Local density is calculated according to the sum of the fractions of both mineral components multiplied with their respective densities.

If after one timestep the temperature of a grid cell exceeds the experimental solidus implemented in this model (Herzberg et al., 2000), the fraction f_{melt} will be released as melt, bringing the temperature back to the solidus by compensating for the loss of latent heat L (set to be constant at 550 $kJ\,kg^{-1}$). With this approach, residue from melting will not necessarily be $C = 0$ harzburgite, because it is only depleted by the amount needed to generate the melt fraction according to temperature overshoot. If the melting occurs above a depth of 600 km, which is thought to be the critical depth below which melt has a negative buoyancy (Ohtani et al., 1998), the entire melt is removed as basaltic crust to the surface and set to surface temperature, thus losing energy $C_P(T_{surf} - T_{solidus})$ per unit mass. In order to calculate the total heat flow due to melting and eruption we use:

$$Q_{erupt} = \dot{M}\big(L + C_P(T_{solidus} - T_{surf})\big),$$

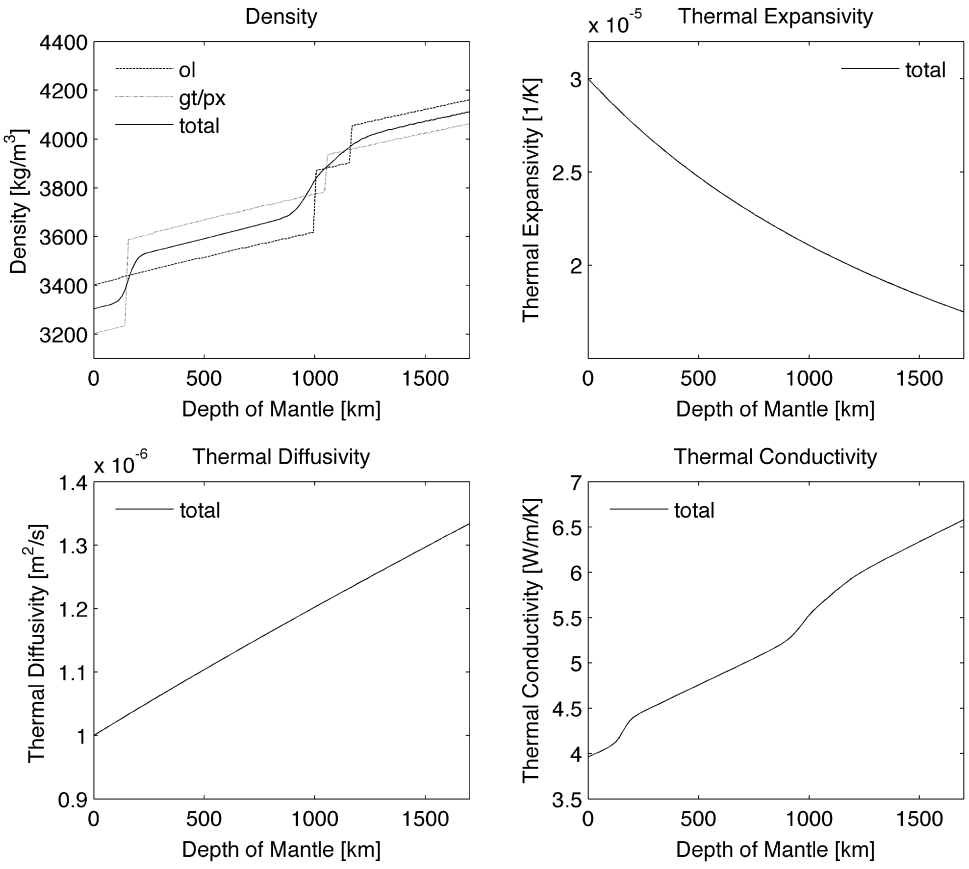

Fig. 1. Adiabatic reference state for the olivine (dashed line) and the garnet–pyroxene (dotted line) system. The total mantle density ρ varies from 3304 kg m^{-3} at the surface to 4113 kg m^{-3} at the CMB; thermal expansivity α varies from 3×10^{-5} to 1.8×10^{-5} K^{-1}; thermal diffusivity κ from 1×10^{-6} to 1.33×10^{-6} m^2/s; thermal conductivity k from 3.96 to 6.58 W m^{-1} K^{-1}.

where $\dot{M}$ is the mass flux through melting and eruption generated per unit time, L is the latent heat per unit mass and $C_P(T_{\text{solidus}} - T_{\text{surf}})$ the heat loss representing the fast radiative heat loss of hot erupted melts exposed on the surface per unit mass.

One drawback of instant eruption of all the generated melt is that it will slightly overestimate the thermal impact of eruption heat flux. A more realistic treatment would account for heat transported into the lithosphere by intrusions, since a certain percentage of melt will get stuck on the way to the surface. This has for the moment been neglected for simplicity, but will be a major focus in future studies on melting/eruption treatment, which will also involve more systematic sampling of the parameter space concerned. If melt is intruded into the crust rather than erupted, its latent heat is still removed from the source region and so the first term in the heat loss equation remains unchanged. In case of intrusion, however, the second term (excess thermal energy) is not needed. Instead of immediately radiating energy to space, the surrounding crust is heated up, thus altering the geotherm and resulting in higher local surface heat flux. The excess thermal energy delivered by intrusion of melt therefore results in increased heat loss from thermal conduction. To summarize, the effective heat loss through magmatism would probably be similar, but some of it would be counted as conductive heat loss rather than radiative heat loss from surface lava flows. Additionally, a recent study on 2D-models with self-consistent melt propagation prior to eruption has shown that eruption efficiencies are in the order of 80 percent of melt production (O'Neill et al., 2007). Although another study derived eruption efficiencies of only 5–20 percent based on observation on volcanic lava flows (Kiefer, 2003), we are confident that our simplification will not cause dramatic errors in total surface heat flux values, although it will slightly overestimate the thermal impact of melting and eruption on the model evolution.

In their recent study, O'Neill et al. (2007) showed that the choice of the solidus has by far the most sensitive influence on melt production in the model. Therefore we chose our melting model to be well within the physical constraints given by laboratory results. To do so, we use a dry mantle solidus from Herzberg et al. (2000) applied to a reference pressure profile obtained from a SNC-type martian density profile (Bertka and Fei, 1998). The solidus temperature is 1143 °C at 0 GPa, which is at the lower end of constraints obtained in experimental studies ranging from 1100 °C in Bertka and Holloway (1994) up to 1400 °C in Musselwhite et al. (2006). Additionally, the solidus is allowed to react to depletion of the source region by linearly increasing the solidus by up to 60 degrees as C decreased from 0.25 to 0 in the source material (McKenzie and Bickle, 1988). This results in basalt melting out of an almost depleted mantle source at 60 degrees higher than from a fertile source at the same pressure.

Based on geophysical and geochemical constraints as well as on the results of parameterized mantle convection models (Breuer and Spohn, 2006; Hauck and Phillips, 2002), the crustal growth is generally thought to take place largely during the first 500 Myr of the planetary evolution, and the mean crustal thickness to be between 50 and 100 km. Our model prescription measures crustal thickness at the depth where composition is $C = 0.75$. We chose this value based on tests where we inserted a crust of known thickness into the model and then used our algorithm to retrieve the crustal thickness. However, the high value chosen for potential crustal thickness and the instantaneous eruption treatment render it more likely than not, that we will overestimate crustal thick-

Table 2
Phase transition properties for Mars.

i	Minerals	d [km]	T [K]	$\Delta\rho$ [$\frac{kg}{m^3}$]	γ [$\frac{MPa}{K}$]	$\Delta\eta$	w [km]
			Olivine system				
1	β-spinel $\rightarrow$ γ-spinel	1173	1600	150	+5.0	10	85
2	olivine $\rightarrow$ β-spinel	1007	1600	252	+2.5	30	51
			Garnet–pyroxene system				
1	garnet/pyroxene $\rightarrow$ majorite	1055	1600	150	+1.0	40	170
2	basalt $\rightarrow$ eclogite	158	0	350	0	0	34

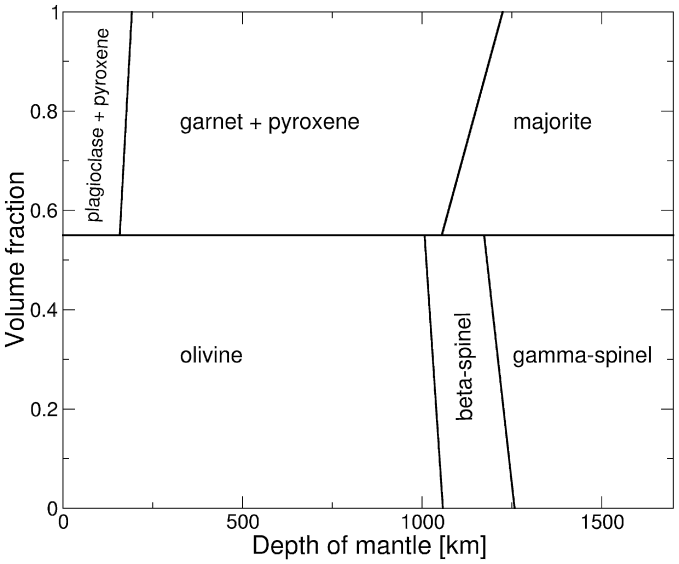

Fig. 2. Simplified mineral phase assemblage used for all model runs performed for this study. The mantle chemistry is generally treated as a two-phase system of olivine and garnet–pyroxene. Corresponding phase transition parameters are to be found in Table 2.

ness in general. Nevertheless, we expect the relative distribution of crustal thickness to still be meaningful for our interpretations.

2.5. Phase transitions

Phase transitions are defined in both the olivine and the garnet-pyroxene fraction of mantle material. Therefore the presence of mineral phases depends on composition and solid–solid phase transitions defined through pressure and temperature by their Clapeyron slopes. The phase transition parameters, derived from the experimentally determined phase diagram for martian mantle composition given by Bertka and Fei (1997), are listed in Table 2. The exact position of every phase change, its deflection due to thermal up- or downwelling and its sharpness are calculated using the phase function

$$\Gamma_{ij} = \frac{1}{2}\left[1 + \tanh\frac{(d - d_{ij}) - \gamma_{ij}(T - T_{ij})}{w_{ij}}\right] \tag{10}$$

with T_{ij} and d_{ij} being the reference temperature and depth of the ith phase transition of the jth mineralogical system, and w_{ij} and γ_{ij} the respective widths and Clapeyron slopes. The width of the phase transitions is set to be between 34 and 170 km to reflect the different nature of the respective mineralogical processes. Whereas garnet and clinopyroxene gradually transform into the majorite structure, resulting in a transition zone rather than a sharp boundary, the olivine to β-spinel transition, for example, is closer to a discrete boundary. Fig. 2 gives a plot of the simplified phase assemblage used in this study.

2.6. Viscosity

Viscosity η strongly depends on temperature and z-coordinate, which is positive in the upward direction:

$$\eta(T, z) = A_\eta \cdot \eta_{\text{ref}} \cdot e^{\frac{E_\eta + (1-z)V_\eta}{T}} \cdot \sum_{ij}[\Delta\eta_{ij}]^{\Gamma_{ij}\cdot f_j}, \tag{11}$$

where the subscripts i and j denote the number and the mineralogical system of the phase transition: $i = 1, 2$ and $j = \text{ol, gt–px}$; Γ_{ij} is the phase function defining mineral fractions as explained above; the viscosity jump $\Delta\eta_{ij}$ will be discussed below. E_η and V_η represent the nondimensional activation energy and activation volume. The values $E_\eta = 200\ \text{kJ mol}^{-1}$ and $V_\eta = 4.5\ \text{cm}^3\,\text{mol}^{-1}$ are chosen to be in a reasonable range for dry olivine (Karato and Jung, 2003), although both of them had to be chosen at the lower end of experimental constraints. The activation energy in our numerical models is constrained by reasons of resolution and numerical stability. The chosen value, however is still high enough to ensure a stable rigid lid. The activation volume, too, has to be comparatively low for our models in order to maintain a viscosity increase of roughly three orders of magnitude once the phase-dependent viscosity jumps are added to the lower mantle. Using the pre-exponential factor A_η, the viscosity is scaled to be $\eta = \eta_{\text{ref}}$ at $T_{\text{ref}} = 1400$ K and $z = z_{\text{ref}} = 1700$ km.

As discussed in the introduction, a mid-mantle viscosity jump provides a powerful mechanism to obtain an effective and short-timescale reduction of convective degree under a rigid lid. In order to not impose such a viscosity layering arbitrarily, a closer look at the mineralogy is necessary. In general, we expect physical properties to change at a mineralogical phase transition. Experimental studies of mantle minerals provide good reason to believe that the crystal structures of majorite-rich garnet and also β- and γ-spinel, the high pressure phases of olivine, should show a significantly higher viscosity than the respective upper mantle phases (Meade and Jeanloz, 1990). Inverse studies of mantle viscosity on Earth lead to a similar conclusion (Forte and Mitrovica, 2001; Mitrovica and Forte, 2004). To simulate this, each phase transition is combined with a viscosity jump using the parameter $\Delta\eta_{ij}$. The size of the viscosity jump added to each phase transition is given in Table 2. Fig. 3 shows the resulting viscosity profile used in our models. The study mentioned above, however, does not state quantitative values of the mineralogical viscosity increase. Since the transition zone in the Earth mantle is almost negligible compared to the influence of the much larger perovskite domain, the usual methods to invert for Earth viscosity profiles are not very sensitive to the viscosity jump at the transition zone (e.g. Kaufmann and Lambeck, 2002). Thus, there is no real data at the moment to safely constrain the amount of viscosity jump expected at the transition zone. Considering this, we take care not to overestimate the influence of the viscosity jumps while still providing good conditions to reduce convective degree. To do so, we select the parameters to be in a range that results in a total viscosity jump of 40 over all phase transitions, which, based on the parameters tested in Roberts and Zhong (2006), is expected to produce one-ridge rather than one-plume convection.

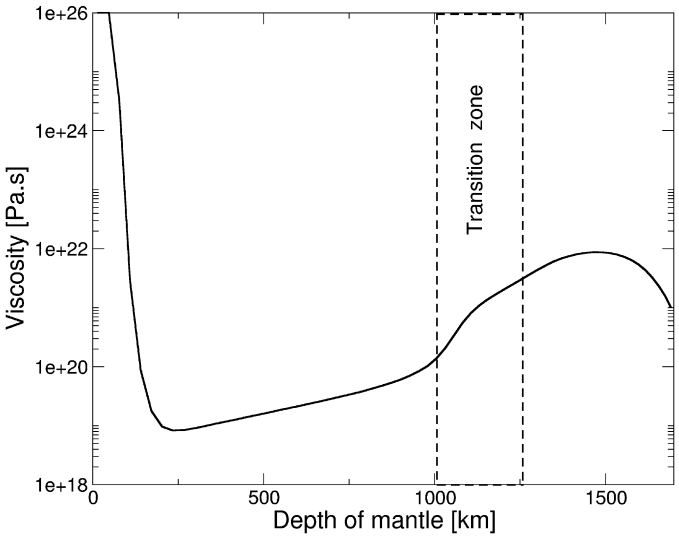

Fig. 3. Reference viscosity profile of all runs. Dashed box marks the martian transition zone in the lower mantle, where occurring phase transitions cause a viscosity increase.

Table 3
List of runs employed in this study.

Case ID	Ra_s	η_{ref} [Pa s]	T_{init} [K]	Melting
REF_NOMELT	3×10^6	1.28×10^{21}	1600	Off
REF_MELT	3×10^6	1.28×10^{21}	1600	On
MID_RA	5×10^6	7.68×10^{20}	1600	On
HIGH_RA/HIGH_TMP	7×10^6	5.48×10^{20}	1600	On
MID_TMP	7×10^6	5.48×10^{20}	1550	On
LOW_TMP	7×10^6	5.48×10^{20}	1500	On

2.7. Method

All cases are computed at a resolution of $96 \times 288 \times 64 \times 2$ grid points, giving a total of 3.54 million cells. The grid is refined at the surface and the mid-mantle phase transitions. Resolution tests show that this resolution is necessary to appropriately model the low viscosity upper mantle dynamics, where melting takes place. To track melting and composition, 50 million tracer particles are needed. Calculations are done on 64 CPUs of a dual Opteron cluster. One model calculation consists of up to 22,000 timesteps and runs for around four full days.

The parameters for the runs performed for this study are listed in Table 3. The runs are organized in two series of three runs. In the first series, the Rayleigh number is increased with an interval of 2×10^6, between $Ra = 3.0 \times 10^6$ and $Ra = 7.0 \times 10^6$. Preliminary cases in 2D indicate that Ra is the parameter with the most significant accelerating effect on the evolution of a degree-1 convection. Even very small changes in Ra are expected to alter the timescale of this process by several 10s of Myrs. In the second series, we study the coupling of initial potential temperature with melting and crust formation by choosing initial temperatures of 1500, 1550 and 1600 K. The narrow parameter range of only 100 K for initial temperature is chosen to demonstrate how crust formation reacts even to rather small differences in early thermal evolution. To quantify the important influence of melting and eruption on thermal evolution of the model, one reference case was computed with melting and differentiation switched off.

With the goal to focus on the earliest episode of martian history, all models are run for 1 Gyr model time.

3. Results

The results of the model runs are presented focusing mainly on the reduction of convective degree with time and on the evolution of crustal thickness distribution in space and with time. Finally, we will briefly discuss the influence of melting and magmatism on the thermal evolution of Mars.

3.1. Reduction of convective degree with time

All models, independent of their Ra, are observed to be dominated by the following two characteristic processes.

Firstly, small-scale downwellings in the form of interconnected sheets drop from beneath the rigid-lid lithosphere into the low viscosity upper mantle. Secondly, quite different from this is the structure of the upwellings. Due to the higher viscosity of the martian transition zone (from 1007 km depth downwards), the dominant wavelength for Rayleigh–Taylor instabilities in the lower mantle is much higher than in the upper mantle, hence the large scale difference of upwelling features compared to downwellings. Mantle upwellings are few but strong, enough to soon overrule the small-scale downwelling geometry in the upper mantle. Downwellings are then collected between strong upwellings and their geometry becomes linearly stretched in shape, aligning with the outwards flow of the plume heads spreading out below the lithosphere.

However, the typical upwelling structures in our models do not satisfy standard circular plume geometry, but rather resemble interconnected, ridge-like structures spanning large regions of the lower mantle. These upwellings rapidly converge into one single ridge, which may transit through a state of near degree two (ring-shaped ridge covering between 270 to a full 360 degrees around the core) and eventually contracts into a sometimes slightly bent ridge of 90 to 120 degrees in length. The intensity of the upwelling, however, is not homogeneous along the ridge, but is concentrated towards both ends, with one end often being more vigorous than the other. The existence of such patterns has already been observed for similar model settings by Roberts and Zhong (2006).

As we will demonstrate below, this convective planform represents an intermediate state between $l = 2$ and $l = 1$ convective degree. We will use the term one-ridge convection introduced above to refer to this specific kind of convective planform. Our models suggest that such convective planforms may be stable for several hundreds of Myrs.

The influence of Ra on the evolution of convective planform found by previous studies (e.g. Roberts and Zhong, 2006) is confirmed by our results. Due to complex time-dependent behavior, no strict scaling law was obtained to describe the reduction of timescale with Rayleigh number for a stable low-degree convection to arise. It is clear, however, that more vigorous convection significantly speeds up all processes leading to a reduction of convective degree. For example, the transition to a subhemispherical ridge-like upwelling takes 125 Myr in the case with highest Ra (HIGH_RA) compared to more than 300 Myr in the reference case with lowest Ra (REF_MELT). Fig. 4 gives four timeframes of the model run HIGH_RA to demonstrate the quick reduction of convective degree and the evolution of a stable one-ridge upwelling.

Fig. 5 gives plots of the relative amplitudes of spherical harmonic degrees with depth for the T-field of the three runs with varying Ra, REF_MELT, MID_RA and HIGH_RA (right column), taken at end time $t = 1$ Gyr. For all three cases, the spectrum is mainly concentrated on $l = 1$ and $l = 2$, as predicted by the shape of the one-ridge upwelling. In this context, an increasing length of the upwelling ridge shifts the spectrum slightly away from $l = 1$ towards $l = 2$. This trend can be followed in these cases, where the lowest Ra (uppermost plot in Fig. 5) results in the longest ridge and also in an almost even distribution of convective degree on $l = 1$ and $l = 2$.

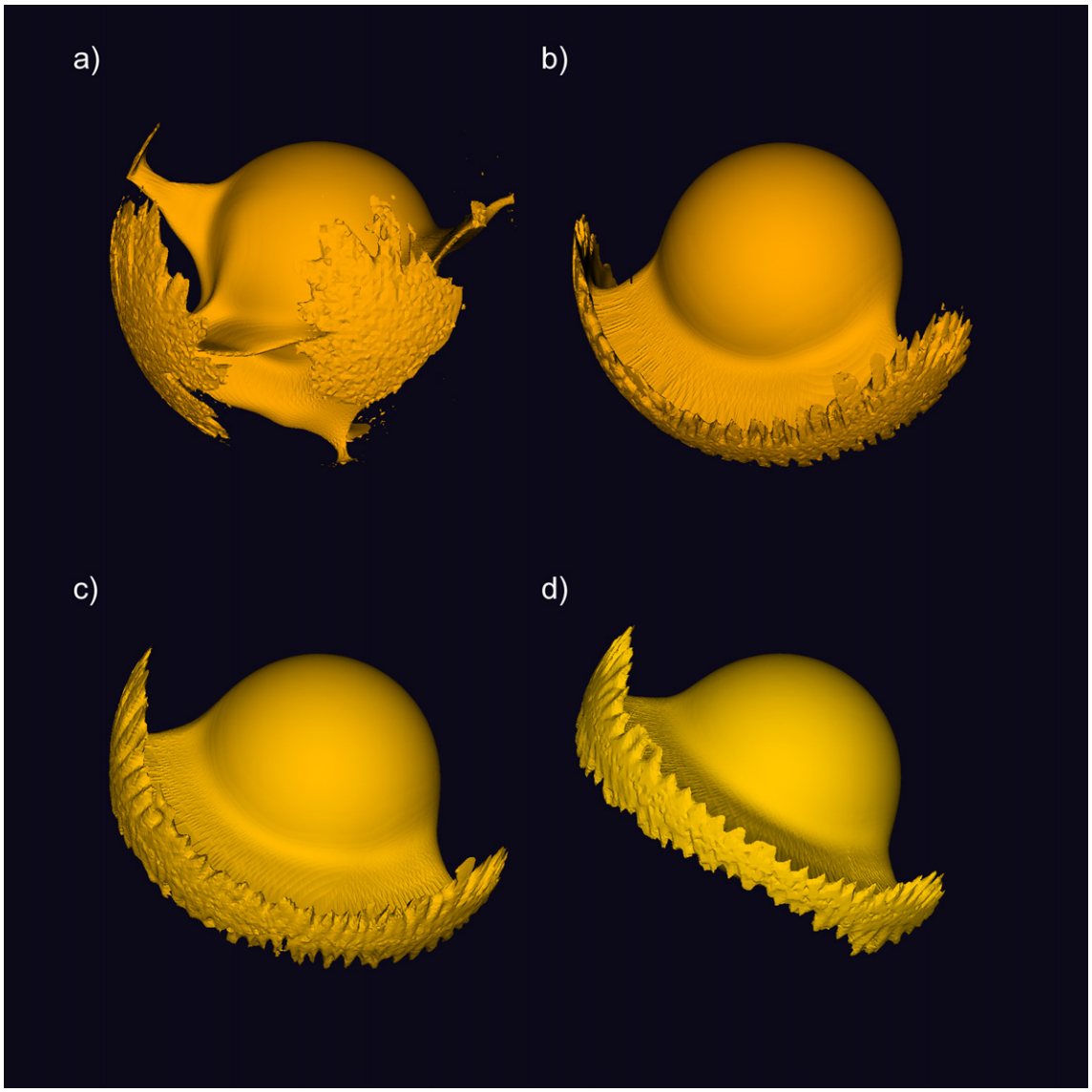

Fig. 4. Four frames at times t of case HIGH_RA. Shown are isosurfaces of temperature T, each taken at a level appropriate to display the upwelling structure of mantle convection. First frame, (a) at $t = 100$ Myrs and $T = 1550$ K, (b) $t = 500$ Myrs and $T = 1520$ K, (c) $t = 750$ Myrs and $T = 1510$ K, and of the final state of the model run at $t = 1$ Gyr and $T = 1500$ K. The typical one-ridge structure of convection is stable in shape but not position over several 100 Myrs. After only 100 Myrs, all upwellings are concentrated into one hemisphere and after 250 Myrs, the one-ridge planform is well established. Note that downwellings cannot be easily displayed because of their small-scale structure. They are not similar in shape to the one-ridge upwelling.

3.2. Crustal thickness distribution

Apart from the spherical harmonics spectrum, Fig. 5 also displays the crustal thickness in a map projection for the same three cases with varying *Ra* (left column of plots). To demonstrate how these patterns of crustal thickness distribution are correlated to underlying convectional features, Fig. 6 shows output frames of both upwelling planform and crustal thickness at 1 Gyr model time of the cases REF_MELT, MID_RA and HIGH_RA. We observe two main crustal signatures in all of the results. Firstly, massive piles of crust often exceeding 100 km in thickness form above major upwellings. These patches of thick crust reflect the shape and intensity of the underlying convective feature. The melting and crust formation at times even extends as far away from the center of the upwelling as the influence of the plume head is the significant feature of mantle flow.

Secondly, we also see a signature of the previously mentioned sublithospheric small-scale convection. The crust produced by this convective feature is found on the entire surface of the planet, starting at the boundaries of plume heads and from there extending out in linear features, spanning over the hemisphere of downwelling. Generally, the geometry of these small-scale convection cells is of an approximately hexagonal geometry, defined by the structure of sheet-like cold downwellings dropping from the rigid lid. In regions close to upwellings, however, these features are extended by mantle flow into linear shapes pointing away from the center of upwelling.

The evolution of mean crustal thickness and eruption rates of all model settings are given in Figs. 7 and 8. The influence of increasing Rayleigh number on crustal production consists largely of an earlier onset and higher melting rates, which leads to a faster depletion and cooling of the source region. This eventually leads to a decrease in melting rates again. The increase in convective vigor with increasing *Ra* also leads to an increasing amount of sublithospheric erosion and crustal recycling. Therefore the mean crustal thickness of the high *Ra* case HIGH_RA in the end is lower than in corresponding lower *Ra* cases REF_MELT and MID_RA. With time, there is an observed decorrelation of the mean crustal thick-

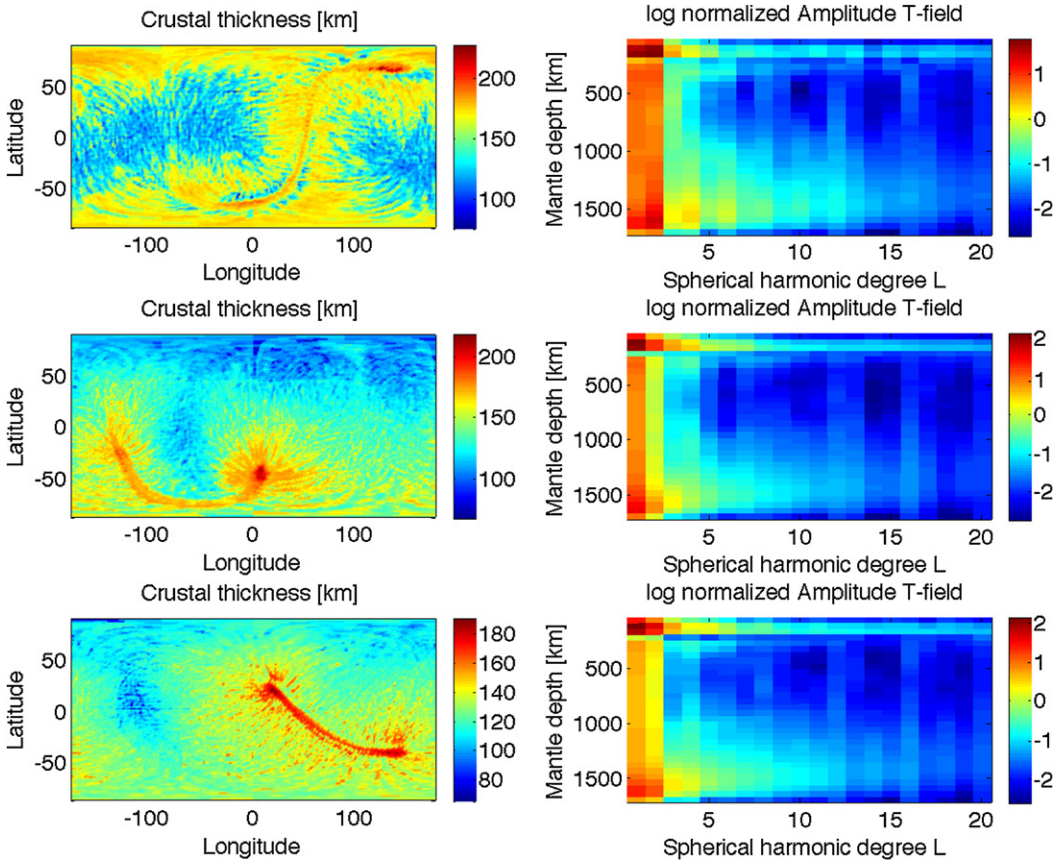

Fig. 5. Crustal thickness map (left) and amplitudes of spherical harmonic degrees $l = 1$–20 of T-field with depth (right) after 1 Gyr for cases with increasing *Ra*. Presented are the model runs REF_MELT (top row), (b) MID_RA (middle row), and (c) HIGH_RA (bottom row). The spectrum of the T-fields displays a high concentration of convective power towards very low degrees of $l = 1$ to $l = 2$. Maps of crustal thickness display elongated patterns of thick crust along the trace of one-ridge upwellings.

ness with respect to eruption rates. Whereas eruption rates reach a stable and slightly decreasing level towards 1 Gyr, the crustal thickness of MID_RA and HIGH_RA reach a saturation level after 800 and 700 Myr, respectively. Where crustal thickness exceeds the thickness of the convective boundary layer (i.e. the thermal thickness of the lithosphere), the lower crust is eroded and recycled into the mantle. Our results confirm the physical expectation that this process is positively correlated to *Ra* and mean T in the mantle.

The influence of initial temperature T_{init} on crustal growth is generally positive, i.e. with increasing T_{init}, melting starts earlier and melting rates are slightly higher during the first 200 Myr. Afterwards, melting rates converge to almost identical levels, leading to similar crustal growth, only distinguishable by a thickness offset of around 24 km between runs with a difference of 50 K in T_{init}. This corresponds to the earlier and more intense onset of magmatic activity. After 800 Myr the difference in mean crustal thickness decreases again to values of around 5 to 10 km.

In general, the overall influence of both *Ra* and T_{init} on mean crustal thickness is rather low. This is not surprising, as with this model configuration, almost all cases reach a saturation level, where the crust does not grow substantially any more and the mean crustal thickness approaches the thickness of the rigid lid, serving as an upper boundary for crustal growth.

3.3. Thermal significance of melting and magmatism

Due to exponential decay of radiogenic heat sources, internal heating in young planets is rather high compared to today's values. With no additional heat removal, a rigid-lid setting would lead to a massive overheating of the mantle. To demonstrate this, we run a reference case with identical setting as REF_MELT, but with melting and eruption switched off. The effect on the thermal evolution is significant, as can easily be observed in Fig. 9 (dash-dotted line). The isolating effect of the conductive lid leads to a fast increase in mean mantle temperature, leading to high convective vigor.

Fig. 10 displays the evolution of mean mantle temperature and CMB heat flow with time for three identical models, where the only changing parameter is initial mantle temperature. Although we start with a step of 50 K in prescribed initial temperature, the difference in mean mantle temperature rapidly decays to values below 1 K after 1 Gyr. The same process is observed for CMB heat flux, which also rapidly converges to a similar value independent of initial temperature.

4. Discussion

4.1. Mantle convection

Up to now, most studies have proposed $l = 1$ convection, i.e. a single plume configuration, to be responsible for the formation of the dichotomy (e.g. Zhong and Zuber, 2001). However, since the dichotomy itself is not circular, but rather elliptical in geometry, similar in shape to the halves of a tennis ball, the one-ridge convective planform obtained in these results might be a better fit to this surface geometry. To generate one-plume structures under a rigid lid, larger viscosity contrasts at the phase transitions, a lower activation volume for viscosity, or else considerably higher *Ra* would have to be applied, whereas more conservative mantle parameters seem to consistently generate ridge-shaped upwellings.

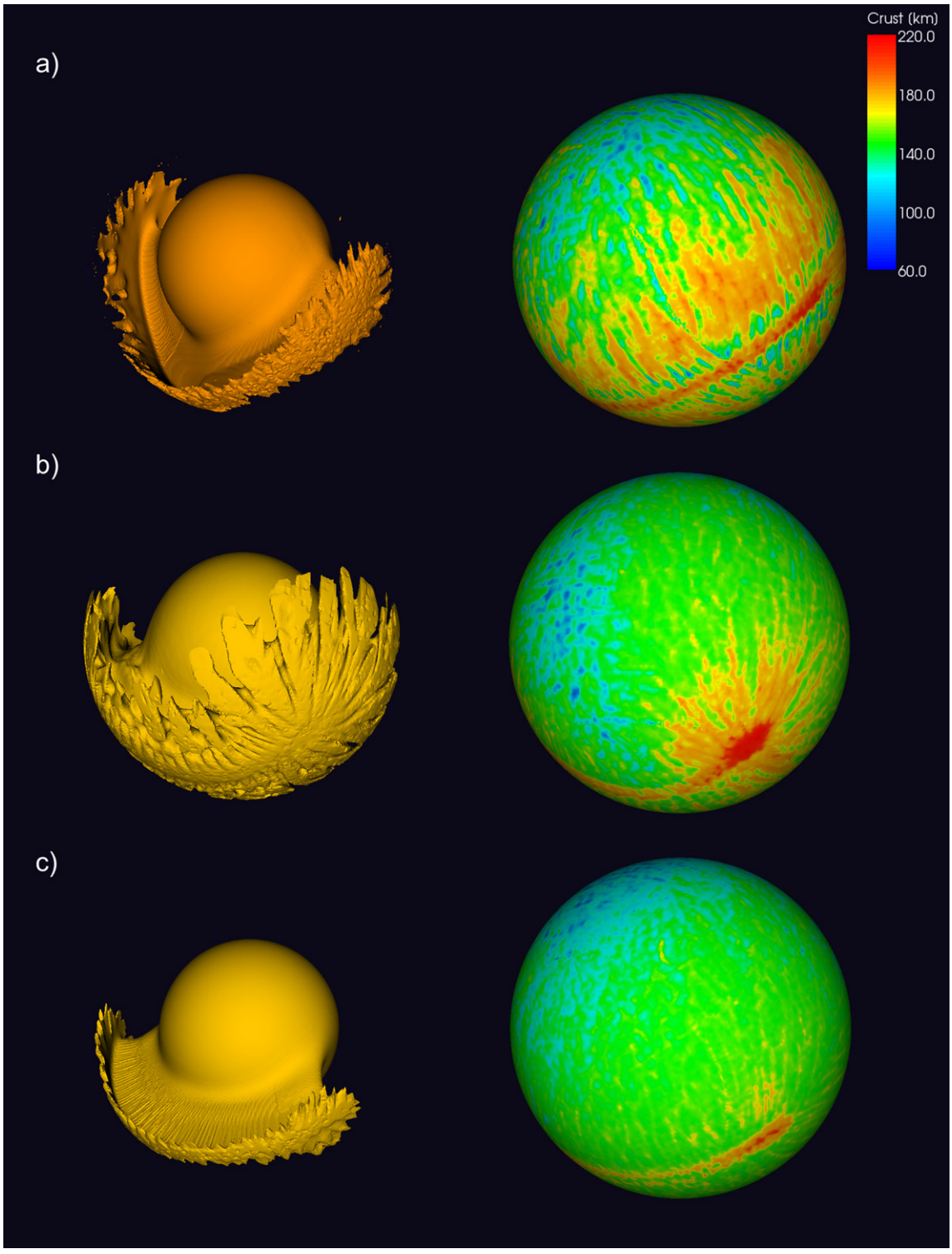

Fig. 6. The model state after 1 Gyr for different *Ra*. Presented are the model runs (a) REF_MELT as isosurface at $T = 1550$ K to the left and corresponding crustal thickness map to the right, (b) MID_RA (isosurface at $T = 1500$ K), and (c) HIGH_RA (isosurface at $T = 1500$ K). The correlation between mantle flow and crustal patterns is clearly visible. Although large-scale upwellings produce the largest amount of crust, a significant component of crustal production also takes place in regions of small-scale sublithospheric convection driven by sheet- and drop-like downwellings.

The mantle convection stays in the rigid-lid regime throughout all of our models. To demonstrate this, horizontally averaged properties are given as radial profiles in Fig. 11. The figure displays radial profiles of viscosity, temperature, horizontal velocity and composition for both the initial timestep (full lines) and the end state after 1 Gyr (dashed lines) of the best fit model HIGH_RA, giving an example of the very similar evolution of these properties in all our model runs. Viscosity and temperature profiles display two main features. Firstly, the CMB temperature is significantly lower at 1 Gyr compared to the initial state, suggesting an efficient core cooling. This will be discussed into more detail below. Secondly, we observe that the average thickness of the thermal lithosphere does not change significantly. Together with the fact that the radial profile of horizontal velocity shows no movement within the lithosphere this confirms the expectation, that the rigid lid is perfectly stable in our models. The depth of no horizontal

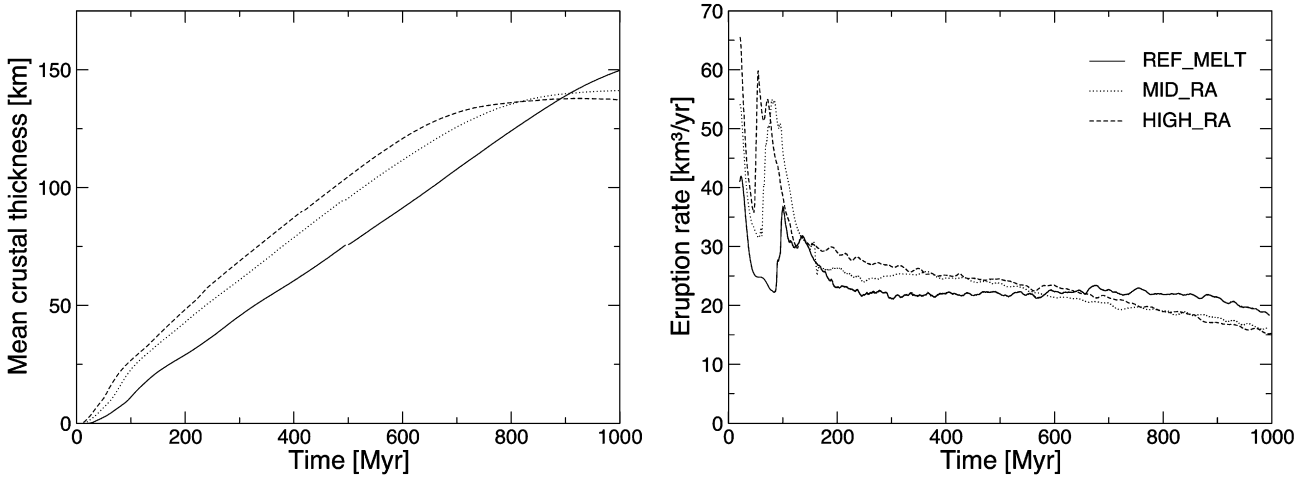

Fig. 7. Time evolution of mean crustal thickness (left) and eruption rate (right) with time for runs with different *Ra*. Case REF_MELT is shown as full, MID_RA as dotted and HIGH_RA as dashed lines. Note that 1 km^3 of crust per year is equivalent to adding a uniform layer of 6.88 mm thickness to the planet's surface.

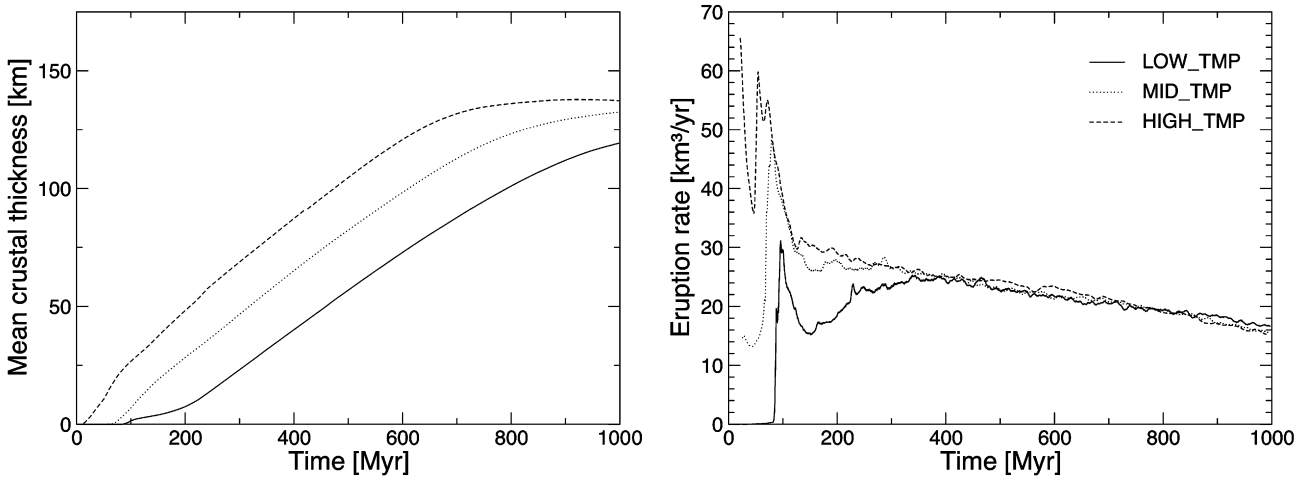

Fig. 8. Time evolution of mean crustal thickness (left) and eruption rate (right) with time for runs with different initial T. Case LOW_TMP is shown as full, MID_TMP as dotted and HIGH_TMP as dashed lines. Note that HIGH_TMP corresponds to the highest *Ra* case in Fig. 7.

motion $D_{\text{lith}} = 145$ km is marked with a gray area in all subfigures as a proxy for the thickness of the lithosphere. The radial profiles of composition show a sharp transition from $C = 1$ within the lithosphere to $C = 0.1333$ throughout the mantle.

Since a planet in the rigid-lid regime does not show significant horizontal motion within the lithosphere, another explanation has to be found for observed migration of magmatic centers on Mars. A recently proposed solution to this problem suggests that differential rotation of the lithosphere is likely to occur where a degree-one convection coexists with a rigid lid (Zhong, 2009). The same effect is observed in our models. The center of magmatism constantly moves against the lithosphere in a rotational type of motion, thus yielding a mechanism to potentially model both the dichotomy and Tharsis in a unified modeling framework.

This study demonstrates the possibility of developing a convective planform fitting the shape of the dichotomy without using any external or internal forcings such as giant impacts (Marinova et al., 2008; Nimmo et al., 2008; Andrews-Hanna et al., 2008), magma ocean overturns (Elkins-Tanton et al., 2005, 2003) or an early transient superplume due to a superheated core (Ke and Solomatov, 2006). The small-scale downwellings due to the rigid lithosphere do not hinder fast reduction of convective degree in our models. Additionally, small-scale convectional melting related to these downwellings provides a possible mechanism to form crust not only above major upwellings, but also on the hemisphere of downwelling. Therefore there do not seem to be any major reasons to reject a purely internally driven origin of the global crustal thickness distribution of Mars.

As mantle viscosity strongly depends on temperature, any temperature changes influence the convective vigor, e.g. higher initial temperatures reduce the initial viscosity of the mantle and thus have a similar effect to a slight increase in *Ra*. The overall evolution of convective vigor, and coupled to it, the timescale needed to obtain low-degree convection is therefore strongly linked to the thermal evolution of the mantle This again is strongly influenced by magmatic activity, as will be discussed below.

4.2. Crust formation

The crustal structures arising from low-degree convection largely follow our expectations. There are two processes leading to melting in the upper mantle. By far the most melt is produced by decompression melting above large mantle upwellings. Since upwellings are few but strong in our models, melting and eruption correspondingly reach very high values in upwelling regions. Therefore, the thickest crust is consistently found as large piles above major upwellings. With one-ridge convection, upwellings are not stable plumes but time-dependent ridge-shaped structures. Our models are capable of producing massive crustal thickness limited to a region roughly elliptical in shape on a timescale of less

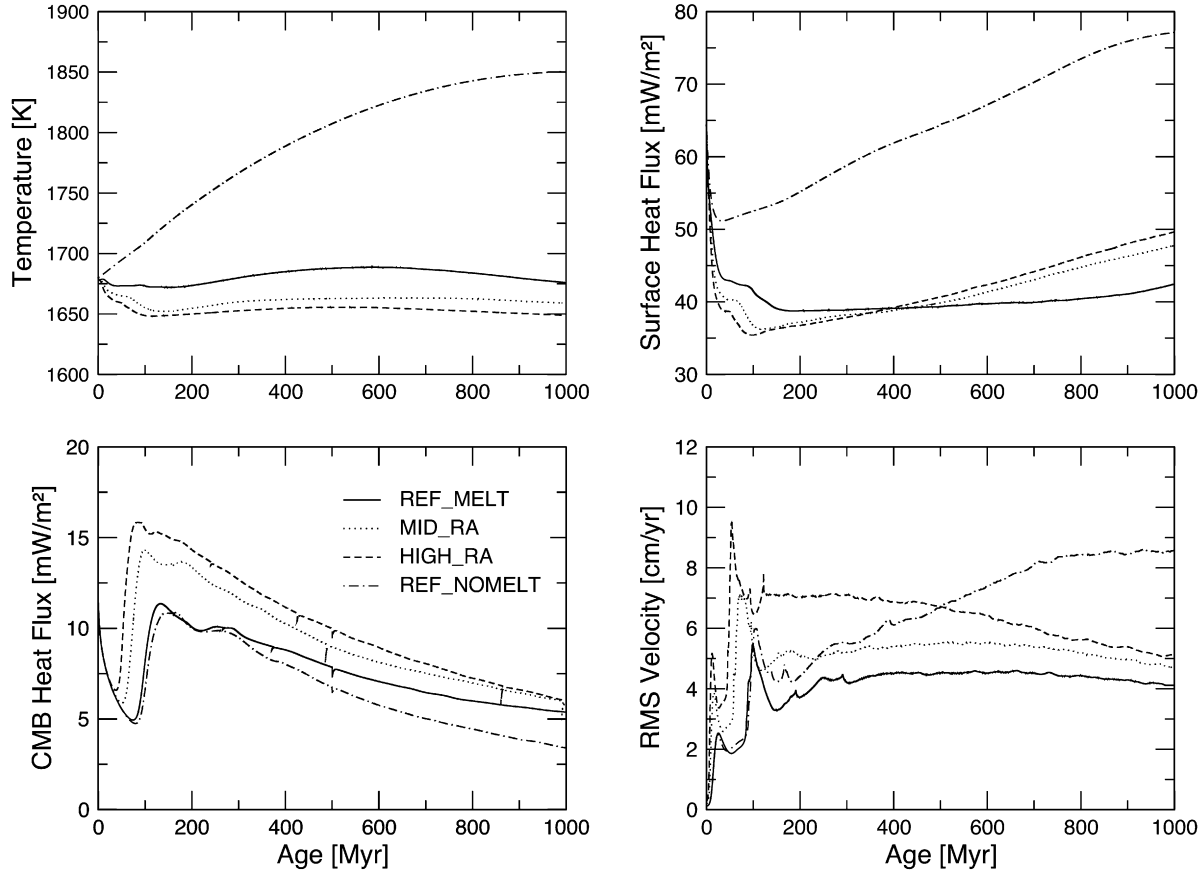

Fig. 9. Time evolution of runs with different *Ra* and reference case without melting. Evolution of mean mantle temperature, surface and CMB conductive heat flux and RMS velocity for case REF_MELT is shown as full, MID_RA as dotted, HIGH_RA as dashed and REF_NOMELT as dash-dotted lines.

then 300 Myr. Thus, our results fulfill some of the available geological and geophysical constraints on martian mantle dynamics and crust formation. Although some timing issues are still unresolved — during early Hesperian, surface magmatism should cease on the southern hemisphere, while it persists longer on the northern hemisphere, Tharsis and Elysium — this scenario still seems to offer a possible origin of the southern highland crust.

The second melting process, however, occurs where small-scale downwellings are the dominant features of convection in the sublithospheric mantle. In these regions, small-scale convection melting occurs, producing a much thinner crust. Linear crustal features usually stretch away from upwellings and cover all the planet's surface other than the regions of major upwellings. The small-scale sublithospheric features of mantle flow resemble those found beneath moving oceanic plates in Earth as has recently been studied by Ballmer et al. (2007). This process shows some potential to explain the Noachian basement crust as well as the late Noachian to early Hesperian ridged plains volcanism proposed based on the morphological evidence found on the northern hemisphere (Frey et al., 2002; Head, 2002).

As previously stated, the model values of mean crustal thickness should be treated with caution due to the various assumptions applied to the description of this quantity in our models. Therefore, we will focus more on the evolution of relative crustal thickness with time, rather than on absolute values. Mean crustal thicknesses of our results after 1 Gyr range from 120 to 150 km, which exceeds estimates obtained by inverting MOLA gravity and topography data giving a mean crustal thickness of the order of 50 km (Neumann et al., 2004). Although one test case, which has been run for a longer time, suggests that in the further course of the model, some of the thickest parts of the crust get eroded, the values obtained in our models are still rather high. The most straightforward way to avoid high crustal thickness would be to reduce the fraction of meltable mantle material (gt/px). This could be justified by the likely assumption that the martian mantle was not primitive anymore at the time relevant to the dichotomy formation. During core formation, a considerable amount of melt could already have been extracted from the mantle, rendering it less fertile for later crust formation. This is supported by the results of a recently submitted study on numerical modeling of terrestrial core formation, implying that thermal effects of core formation could lead to widespread melting in the mantle region of a Mars-sized planet (Golabek et al., 2009). How this effect should be scaled for Mars is subject to more refined studies on coupled models of core formation, mantle convection and magmatism that are currently in progress.

To quantitatively compare relative crustal distribution to Mars data, Fig. 12 shows histograms of crustal thickness distributions obtained with a sampling bin of 2 km. The plot to the lower right side shows the histogram inverted from MOLA gravity and topography by Neumann et al. (2004). Easily visible is the dichotomous structure of crustal thickness on Mars with one peak at 56 km (southern highlands) and another one at 30 km (northern lowlands). Comparing this to our results, some similar features are visible. Although our results show a consistent positive offset in absolute crustal thickness, the dichotomous structure of our best fit crustal distribution (upper right plot in Fig. 9) is very distinct. The two peaks are positioned at 148 and 122 km, respectively. These values exceed the crustal thicknesses derived from MOLA data. However, the relative position of the two peaks show the same step of 26 km as in the MOLA inversion. The relative structure of at least one of our models therefore is a good first order fit

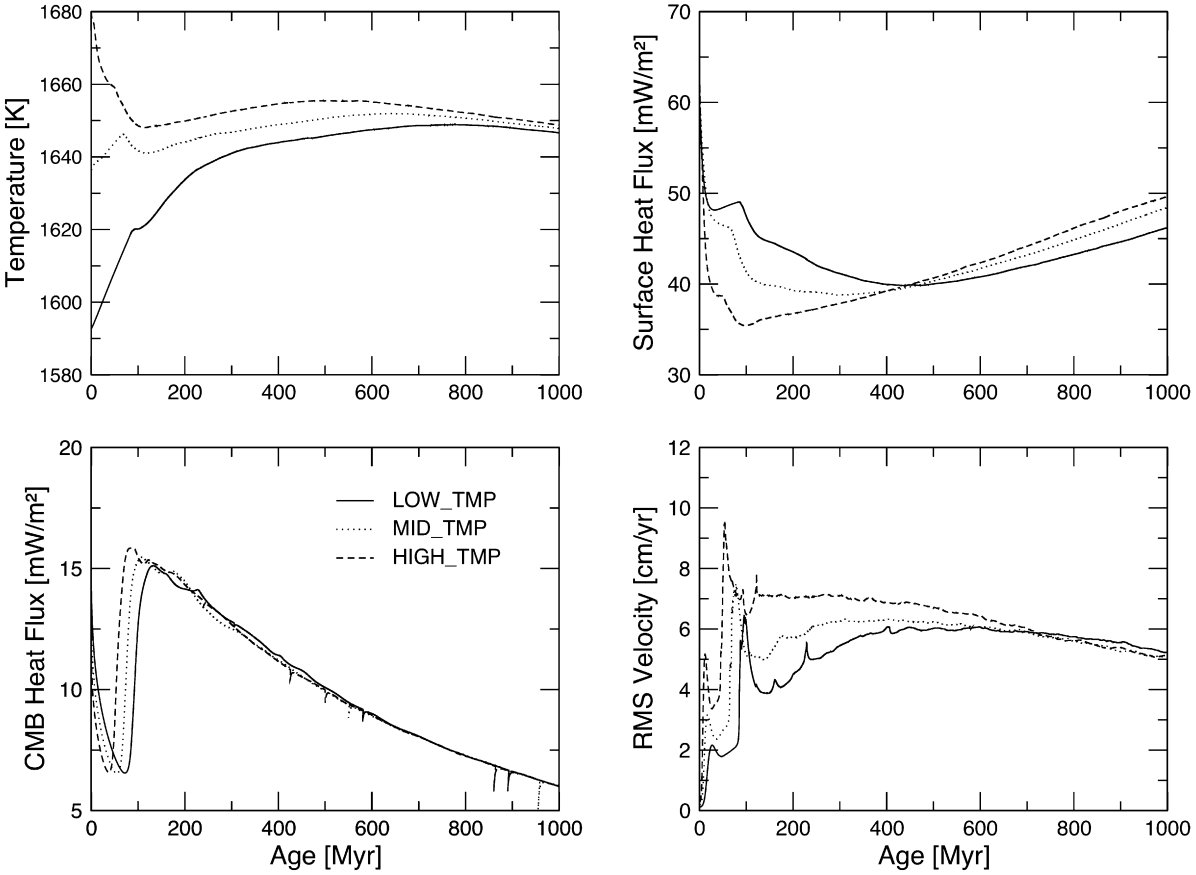

Fig. 10. Time evolution of runs with different initial temperature. Evolution of mean mantle temperature, surface and CMB conductive heat flux and RMS velocity for case LOW_TMP is shown as full, MID_TMP as dotted and HIGH_TMP as dashed lines. Note that HIGH_TMP corresponds to the highest *Ra* case of series 1 in Fig. 9.

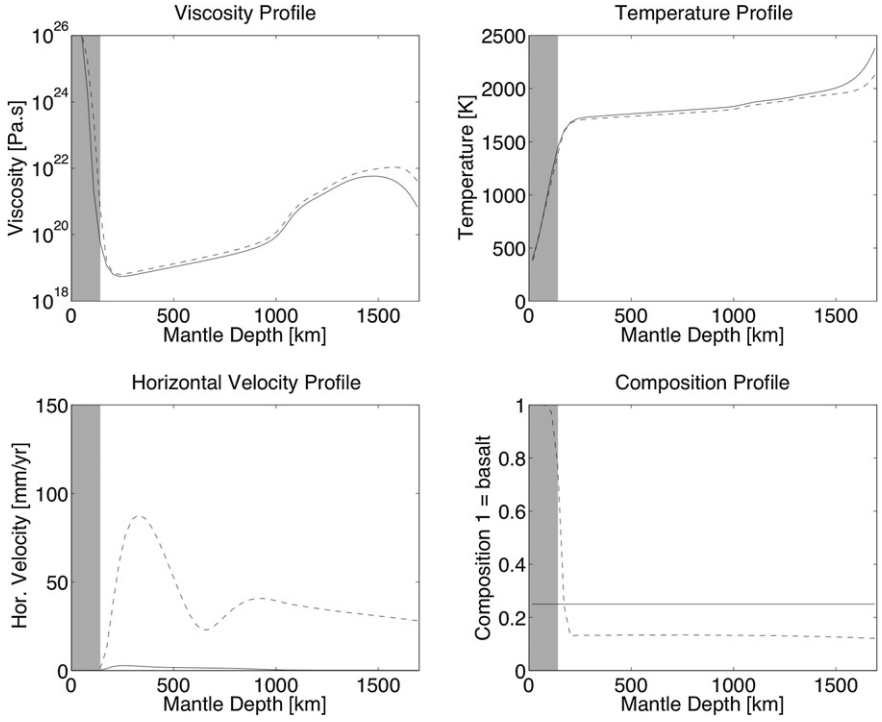

Fig. 11. Horizontally averaged properties for case HIGH_RA, displaying viscosity (upper left), temperature (upper right), horizontal velocity (lower left) and composition (lower right) as profiles against mantle depth. The radial profiles are given at the beginning of the model run at $t = 0$ Gyr (full lines) and $t = 1$ Gyr (dashed lines). The gray areas in each subfigure mark the thickness of the rigid lid at the end of the model run, measured as the region with no horizontal motion (145 km).

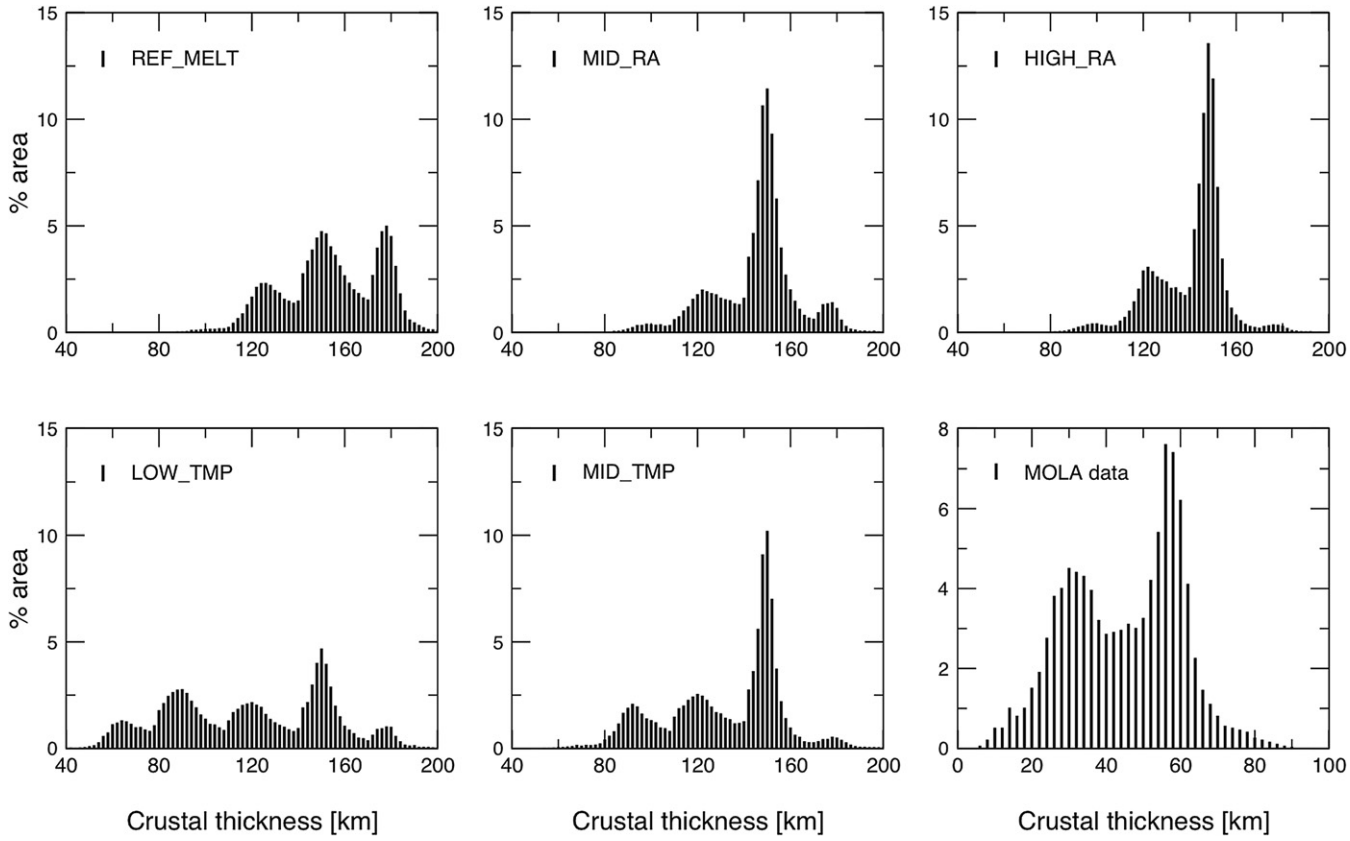

Fig. 12. Histogram of crustal thickness. Crustal thickness is sampled in a bin size of 2 km. To compare our result to Mars data, a histogram obtained from MOLA crustal thickness model is displayed at the lower right side (Neumann et al., 2004). Our best fit model HIGH_RA is to be found on the upper right side. Note, that although absolute thickness is overestimated, the relative spacing of the two peaks is almost identical with a value of 26 ± 2 km.

to the actual relative crustal thickness distribution found on Mars today.

4.3. Thermal evolution

Due to high initial values of the internal heating rate, more heat is released into the mantle than can be conducted through the stagnant lid. This leads to an increase in mean mantle temperature, which affects convective vigor through the T-dependence of viscosity. More vigorous convection leads to more decompression melting by more efficiently bringing hot material from the deep mantle, thus enhancing melt formation. Therefore, higher initial temperatures lead to higher melting rates during the period preceding the development of one-ridge convection, thus leading to higher initial crustal thickness, to which the dichotomous structures produced by the ridge are added. It is possible to fit the curves of mean crustal thickness with time (Fig. 8, left plot) on top of each other in the interval of 300 to 600 Myr by simply translating the full and dotted curves upwards. This upward translation is equivalent to adding primordial crust to the model. To fit the curve of case HIGH_TMP, values of 47 km for case LOW_TMP and 22 km for MID_TMP would be required. Under the assumption that the basement crust of the northern hemisphere is composed of Noachian crust, the structure and thickness of the northern lowland basement could possibly yield useful constraints on initial temperature and onset of small-scale convection melting on Mars.

As discussed above, internal heating in rigid-lid planets tends to overheat the mantle. With melting included in the thermal model, however, latent heat consumption locally buffers temperature very efficiently to values around the solidus. All melt produced during one timestep is instantly removed to the surface and set to surface temperature, which acts as a major heat removal mechanism. It is indeed far more efficient than conductive heat removal and can reach values exceeding 200 mW m^{-2} during large melting events. After the first 60 to 100 Myr (depending on *Ra*), values of eruptive heat flux tend to decrease to values comparable with diffusive heat flux.

It now becomes clear that sources and sinks of heat in the partially melting upper mantle together form a self-regulating feedback system. Strong internal heating and consequently more vigorous convection promotes higher melting rates, which again very efficiently removes heat to the surface and therefore damps its own source by reducing the effect of radioactive heating. The system eventually is found in an equilibrium state between internal heating and magmatic cooling. The establishment of this equilibrium appears to be the dominant process in the thermal evolution of our models.

The signatures of an early dynamo in the martian core give us some constraints on CMB heat flux in models of mantle convection (Nimmo and Stevenson, 2000; Connerney et al., 2005). The maximum conductive heat flux out of the martian core is likely to be between 5 and 19 mW m^{-2} (Nimmo and Stevenson, 2000). Whereas it is difficult to satisfy this constraint in a rigid-lid regime without the thermal impact of melting, our models demonstrate that magmatism provides enough cooling to increase CMB heat flux and thus to maintain a core dynamo at least during a short timespan. In our best fit model HIGH_RA (dashed line in Fig. 9), the CMB heat flux reaches values exceeding 15 mW m^{-2} between 80 and 180 Myrs or exceeding 10 mW m^{-2} between 50 and 500 Myrs. Thus a possible core dynamo would exist during the same time as the major part of crust formation takes place in our models. The linear patterns of magnetic reversals discovered on large parts of the southern and some parts of the northern hemisphere (Connerney et al., 1999) could be related to subsequent stages of

time-dependent one-ridge convection, as the geometry of these features coincide with our interpretation of how a one-ridge convective pattern would have been positioned in the mantle to form the dichotomy.

5. Conclusions

The results of this study demonstrate that low-degree convection, especially in a one-ridge planform, produces a crustal structure fitting the martian dichotomy to first order. However, these results also lead to new questions that remain to be investigated, such as the precise influence of melting processes on the heat budget of the planet, the control of various parameters on the mean crustal thickness and the search for realistic ways to model melting and eruption processes, which would govern the shape of a model dichotomy.

As the main findings from this first attempt to self-consistently model the evolution of the martian dichotomy, we can state the following: Firstly, we were able to reproduce models of mantle convection displaying a rapid (120–150 Myr) build up of one-ridge convection under a stable rigid-lid lithosphere. With an improved modeling technique (Tackley, 2008), we were able to handle very large viscosity contrasts and thus apply a realistic viscous rheology. Secondly, we demonstrate that smooth viscosity layering applied to martian type mantle mineralogy proves a vital ingredient to produce one-ridge convection as opposed to one-plume convection.

Our results show that melting and crust formation seems to be the most important way to lose heat on a rigid-lid planet, at least early on. By implementing a simple treatment of self-consistent melting and crustal formation into the models of mantle convection, we were able to track the time evolution of the crustal thickness distribution. The dominant feature of the crustal thickness distribution obtained from one-ridge convection in the mantle is a characteristic, roughly elliptical shape that shows a striking first-order similarity to the shape of the martian dichotomy.

The most important process leading to the formation of this shape is massive decompression melting and time-dependent behavior of the ridge-like upwelling, which in itself can be seen as a link between two superplumes at each end. This configuration allows for the formation of massively thick crust spread over an area comparable to the martian highlands. Furthermore, our results suggest that northern lowland basement crust was formed either shortly before or simultaneously with the southern highlands by means of small-scale convection melting underneath the rigid lid. Although the absolute crustal thickness is overestimated, the relative distribution of crustal thickness shows a good fit to crust models inverted from Mars data. To improve results, more detailed investigations of melting and crust formation will have to be made and igneous intrusion rather than surface eruption will have to be considered.

Acknowledgments

The authors thank James H. Roberts and an anonymous reviewer for careful and constructive comments that helped improving the manuscript. Also, we would like to thank Gregor Golabek and Maxim Ballmer for helpful discussions. Important stimulation for this project also resulted from a series of workshops of the ETH PLANETZ initiative.

References

Andrews-Hanna, J.C., Zuber, M.T., Banerdt, W.B., 2008. The Borealis basin and the origin of the martian crustal dichotomy. Nature 453, 1212–1215.

Ballmer, M., van Hunen, J., Ito, G., Tackley, P.J., Bianco, T.A., 2007. Nonhotspot volcano chains originating from small-scale sublithospheric convection. Geophys. Res. Lett. 34. L23310.

Bertka, C.M., Fei, Y., 1997. Mineralogy of the martian interior up to core–mantle boundary pressures. J. Geophys. Res. 102 (B3), 5251–5264.

Bertka, C.M., Fei, Y., 1998. Density profile of an SNC model martian interior and the moment-of-inertia factor of Mars. Earth Planet. Sci. Lett. (157), 79–88.

Bertka, C.M., Holloway, J.R., 1994. Anhydrous melting of an iron-rich mantle. I. Subsolidus phase assemblages and partial melting phase relationships at 10 to 30 kbar. Contrib. Mineral. Petrol. 115, 313–322.

Breuer, D., Spohn, T., 2006. Viscosity of the martian mantle and its initial temperature: Constraints from crust formation history and the evolution of the magnetic field. Planet. Space Sci. 54, 153–169.

Buffet, B.A., Gable, C.W., O'Connell, R.J., 1994. Linear stability of a layered fluid with mobile surface plates. J. Geophys. Res. 99 (B10), 19885–19900.

Bunge, H.-P., Richards, M.A., Baumgardner, J.R., 1996. Effect of depth-dependent viscosity on the planform of mantle convection. Nature 379, 436–438.

Connerney, J.E.P., Acuna, M.H., Wasilewski, P.J., Ness, N.F., Reme, H., Mazelle, C., Vignes, D., Lin, R.P., Mitchell, D.L., Cloutier, P.A., 1999. Magnetic lineations in the ancient Mars. Science 284, 794–798.

Connerney, J.E.P., Acuna, M.H., Ness, N.F., Kletetschka, G., Mitchell, D.L., Lin, R.P., Reme, H., 2005. Tectonic implications of Mars crustal magnetism. Proc. Natl. Acad. Sci. USA 102 (42), 14970–14975.

Elkins-Tanton, L.T., Parmentier, E.M., Hess, P.C., 2003. Magma ocean fractional crystallization and cumulate overturn in terrestrial planets: Implications for Mars. Meteorit. Planet. Sci. 38 (12), 1753–1771.

Elkins-Tanton, L.T., Hess, P.C., Parmentier, E.M., 2005. Possible formation of ancient crust on Mars through magma ocean processes. J. Geophys. Res. 110. E12S01.

Forte, A.M., Mitrovica, J.X., 2001. Deep-mantle high-viscosity flow and thermochemical structure inferred from seismic and geodynamic data. Nature 410, 1049–1056.

Frey, H., Schultz, R.A., 1988. Large impact basins and the mega-impact origin for the crustal dichotomy on Mars. Geophys. Res. Lett. 15, 229–232.

Frey, H., Roark, J.H., Shockey, K.M., Frey, E.L., Sakimoto, S.H.E., 2002. Ancient lowlands on Mars. Geophys. Res. Lett. 29. 1384.

Golabek, G., Gerya, T.V., Kaus, B.J.P., Ziethe, R., Tackley, P.J., 2009. Rheological controls on the terrestrial core formation mechanism. Geochem. Geophys. Geosyst., submitted for publication.

Harder, H., 1998. Phase transitions and the three-dimensional planform of thermal convection in the martian mantle. J. Geophys. Res. 103 (E7), 16775–16797.

Harder, H., Christensen, U.R., 1996. A one-plume model of martian mantle convection. Nature 380, 507–509.

Hartmann, W.K., 1973. Martian cratering, 4, Mariner 9 initial analysis of cratering chronology. J. Geophys. Res. 78, 4096–4116.

Hauck, S.A., Phillips, R.J., 2002. Thermal and crustal evolution of Mars. J. Geophys. Res. 107 (E7). 5052.

Head, J.W.I., Kreslavsky, M.A., Pratt, S., 2002. Northern lowlands of Mars: Evidence for widespread volcanic flooding and tectonic deformation in the Hesperian Period. J. Geophys. Res. 107. E15003.

Herzberg, C., Raterron, P., Zhang, J., 2000. New experimental observations on the anhydrous solidus for peridotite KLB-1. Geochem. Geophys. Geosyst. 1, doi:10.1029/2000GC00089.

Kageyama, A., Sato, T., 2004. "Yin–Yang grid": An overset grid in spherical geometry. Geochem. Geophys. Geosyst. 5, doi:10.1029/2004GC000734. Q09005.

Karato, S.-I., Jung, H., 2003. Effects of pressure on high-temperature dislocation creep in olivine. Philos. Mag. 83 (3), 401–414.

Kaufmann, G., Lambeck, K., 2002. Glacial isostatic adjustment and the radial viscosity profile from inverse modeling. J. Geophys. Res. 107 (B11). 2280.

Ke, Y., Solomatov, V.S., 2006. Early transient superplumes and the origin of the martian crustal dichotomy. J. Geophys. Res. 111. E10001.

Kiefer, W.S., 2003. Melting in the martian mantle: Shergottite formation and implications for present-day mantle convection on Mars. Meteorit. Planet. Sci. 39 (12), 1815–1832.

Marinova, M.M., Aharonson, O., Asphaug, E., 2008. Mega-impact formation of the Mars hemispheric dichotomy. Nature 453, 1216–1219.

McKenzie, D., Bickle, M.J., 1988. The volume and composition of melt generated by extension of the lithosphere. J. Petr. 29 (3), 625–679.

Meade, Ch., Jeanloz, R., 1990. The strength of mantle silicates at high pressures and room temperature: Implications for the viscosity of the mantle. Nature 348, 533–535.

Mitrovica, J.X., Forte, A.M., 2004. A new inference of mantle viscosity based upon joint inversion of convection and glacial isostatic adjustment data. Earth Planet. Sci. Lett. 225, 177–189.

Musselwhite, D.S., Dalton, H.A., Kiefer, W.S., Treimann, A.H., 2006. Experimental petrology of the basaltic Shergottite Yamato 980459: Implications for the thermal structure of the martian mantle. Meteorit. Planet. Sci. 41, 1271–1290.

Nakagawa, T., Tackley, P.J., 2005. Deep mantle heat flow and thermal evolution of Earth's core in thermo-chemical multiphase models of mantle convection. Geochem. Geophys. Geosyst. 6. Q08003.

Neumann, G.A., Zuber, M.T., Wieczorek, M.A., McGovern, P.J., Lemoine, F.G., Smith, D.E., 2004. Crustal structure of Mars from gravity and topography. J. Geophys. Res. 109. E08002.

Nimmo, F., Stevenson, D.J., 2000. Influence of early plate tectonics on the thermal evolution and magnetic field of Mars. J. Geophys. Res. 105 (E5), 11969–11979.

Nimmo, F., Tanaka, K.L., 2005. Early crustal evolution of Mars. Annu. Rev. Earth Planet. Sci. 33, 133–161.
Nimmo, F., Hart, S.D., Korycanksy, D.G., Agnor, C.B., 2008. Implications of an impact origin for the martian hemispheric dichotomy. Nature 453, 1220–1223.
Ohtani, E., Suzuki, A., Kato, T., 1998. Flotation of olivine and diamond in mantle melt at high pressure: Implications for fractionation in the deep mantle and ultradeep origin of diamond. In: Manghnani, M.H., Yagi, T. (Eds.), Properties of Earth and Planetary Materials at High Pressure and Temperature. In: Geophysical Monographs, vol. 101. AGU, Washington, pp. 227–239.
O'Neill, C., Lenardic, A., Jellinek, A.M., Kiefer, W.S., 2007. Melt propagation and volcanism in mantle convection simulations, with application for martian volcanic and atmospheric evolution. J. Geophys. Res. 112. E07003.
Ramberg, H., 1967. Fluid dynamics of layered systems in the field of gravity, a theoretical basis for certain global structures and isostatic adjustment. Phys. Earth Planet. Int. 1 (2), 63–87.
Roberts, J.H., Zhong, S., 2006. Degree-1 convection in the martian mantle and the origin of the hemispheric dichotomy. J. Geophys. Res. 111. E06013.
Sleep, N.H., 1994. Martian plate tectonics. J. Geophys. Res. 99 (E3), 5639–5655.
Sohl, F., Spohn, T., 1997. The interior structure of Mars: Implications from SNC meteorites. J. Geophys. Res. 102 (E1), 1613–1635.
Steinbach, V., Yuen, D.A., 1994. Effects of depth-dependent properties on the thermal anomalies produced in flush instabilities from phase transitions. Phys. Earth Planet. Int. 86, 165–183.
Tackley, P.J., 1996a. On the ability of phase transitions and viscosity layering to induce long wavelength heterogeneity in the mantle. Geophys. Res. Lett. 23 (15), 1985–1988.
Tackley, P.J., 1996b. Effects of strongly variable viscosity on three-dimensional compressible convection in planetary mantles. J. Geophys. Res. 101 (B2), 3311–3332.
Tackley, P.J., 2008. Modeling compressible mantle convection with large viscosity contrasts in a three-dimensional spherical shell using the Yin–Yang grid. Phys. Earth Planet. Int. 107, 7–18, doi:10.1016/j.pepi.2008.08.005.
Wänke, H., Dreibus, G., 1994. Chemistry and accretion of Mars. Philos. Trans. R. Soc. London (349), 2134–2137.
Watters, T.R., Leuschen, C.J., Plaut, J.J., Picardi, G., Safaeinili, A., Clifford, S.M., Farrell, W.M., Ivanov, A.B., Phillips, R.J., Stofan, E.R., 2006. MARSIS radar sounder evidence of buried basins in the northern lowlands of Mars. Nature 444, 905–908.
Wilhelms, D.E., Squyres, S.W., 1984. The martian hemispheric dichotomy could be due to a giant impact. Nature 309, 138–140.
Wise, D.U., Golombek, M.P., McGill, G.E., 1979. Tectonic evolution of Mars. J. Geophys. Res. 84, 7934–7939.
Xie, S., Tackley, P.J., 2004. Evolution of U-Pb and Sm–Nd systems in numerical models of mantle convection and plate tectonics. J. Geophys. Res. 109. B11204.
Yoshida, M., Kageyama, A., 2006. Low-degree mantle convection with strongly temperature- and depth-dependent viscosity in a three-dimensional spherical shell. J. Geophys. Res. 111, doi:10.1029/2005JB003905. B03412.
Zhong, S., 2009. Migration of Tharsis volcanism on Mars caused by differential rotation of the lithosphere. Nat. Geosci. 2, 19–23.
Zhong, S., Zuber, M.T., 2001. Degree-1 mantle convection and the crustal dichotomy on Mars. Earth Planet. Sci. Lett. 189, 75–84.
Zuber, M.T., 2001. The crust and mantle of Mars. Nature 412, 220–227.